Structural biology with carbon nanotube AFM probes

Adam T Woolley, Chin Li Cheung, Jason H Hafner and Charles M Lieber

Carbon nanotubes represent ideal probes for high-resolution structural and chemical imaging of biomolecules with atomic force microscopy. Recent advances in fabrication of carbon nanotube probes with sub-nanometer radii promise to yield unique insights into the structure, dynamics and function of biological macromolecules and complexes.

Department of Chemistry and Chemical Biology, Harvard University, 12 Oxford Street, Cambridge, MA 02138, USA

Correspondence: Charles M Lieber
E-mail: cml@cmliris.harvard.edu

Keywords: Atomic force microscopy; Carbon nanotube; Chemical imaging; Macromolecule; Structural biology

Received: **27 June 2000**
Revisions requested: **18 July 2000**
Revisions received: **24 August 2000**
Accepted: **15 September 2000**

Published: **28 September 2000**

Chemistry & Biology 2000, **7**:R193–R204

1074-5521/00/$ – see front matter

PII: S1074-5521(00)00037-5

Introduction

The determination of structure–function relationships in biological macromolecules is central to elucidating biochemical pathways, and thereby designing new drugs and understanding their mode of action. Structural biology has played and will continue to play a key role in these endeavors because protein function is closely tied to three-dimensional structure. The workhorse tools of structural biology, X-ray diffraction, electron diffraction and NMR, can almost routinely be used to determine atomic resolution structure of single proteins. Continued advances in these methods are pushing the limits of the size and complexity of systems that can be characterized [1–6], although in the future, expanded needs for biomolecular structure analysis are expected in several areas, including: (1) increased throughput to characterize new gene products discovered by genomic DNA sequencing [7]; (2) routine analysis of multimeric protein–protein and protein–nucleic acid structures involved in, for example, signaling and gene regulation; and (3) elucidation of dynamic processes in these multimeric systems. It is unlikely that the conventional structural tools will meet all of these needs, both because of the increased difficulty of crystallizing large signaling and regulatory protein complexes, which will limit diffraction methods, and the challenges of using solution NMR for large biomolecular systems [8].

Atomic force microscopy (AFM) in biology

Future progress in understanding complex processes in biological systems will clearly require additional, perhaps revolutionary techniques for structural analysis. AFM [9] is one technique with the potential to probe both structure and dynamics of large macromolecular systems, since it permits direct visualization of individual biological structures in vitro [10,11]. The potential for AFM to impact structural biology has been suggested by beautiful images of, for example, two-dimensional arrays of proteins with 'sub-molecular resolution' [10,11], although such captivating data are not without limitations. These shortcomings, which if overcome could dramatically extend the applicability of AFM to structural biology, can be understood by reviewing the key features of an AFM (Figure 1a). Common to all AFMs are an integrated cantilever-tip assembly, a detector to measure cantilever displacement as the sample is scanned, and electronics to acquire and display images. The basic features of AFM and methods of imaging have been reviewed recently [12].

Central to reproducible high-resolution characterization of biological macromolecules with AFM – especially new systems not crystallographically characterized – is the size and shape of the probe tips used for imaging. For example, comparison of a 5 nm radius tip, which corresponds to the typical lower limit of commercial Si probes, and the moderate sized protein GroES highlights the blunt nature of typical tips used in AFM. Commercial tip radii are thus inconsistent with the 'sub-molecular resolution' reported for two-dimensional crystals [13]. This unexpected high resolution has been attributed to sharp asperities [14], although independent characterization of asperities, for ex-

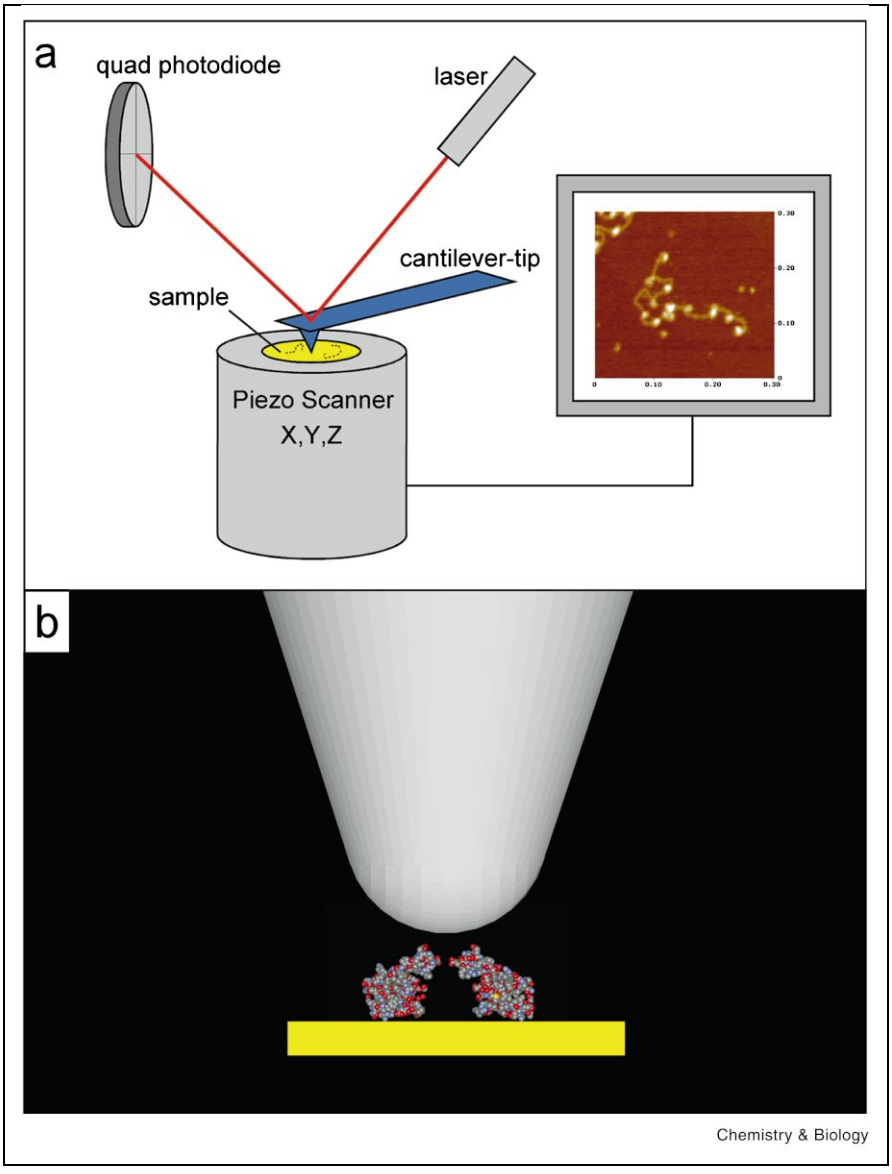

Figure 1. Schematic of an atomic force microscope. **(a)** The cantilever-tip assembly, piezoelectric tube scanner, optical deflection system and computer image are depicted. **(b)** Comparison of a cone-shaped, 5 nm radius of curvature tip and a cross-section of an individual GroES molecule.

ample by transmission electron microscopy (TEM), has not been performed. In addition, microfabricated commercial tips exhibit significant tip-to-tip variability, which further complicates structural studies of new systems in an unbiased manner. Lastly, it is often difficult to attach molecules to commercial probes in a well-defined manner [15], and even when the attachment uses well-defined chemistry like self-assembled monolayers (SAMs) [16], the spatial location of the probe molecules is not known on the <10 nm scale. This limitation has precluded molecular scale functional imaging with AFM.

Hence, one expects that significant advances could be achieved by overcoming the tip limitations outlined above. In particular, an ideal probe tip should have (i) a sub-nanometer radius, (ii) a zero degree cone angle, (iii) mechanical and chemical robustness, and (iv) the potential for molecularly precise modification of the tip end. Moreover, it should be possible to prepare such tips reproducibly with the same features, such that the resolution and other imaging characteristics are predictable, as is the case in diffraction experiments. Is it possible to create and implement the ideal tip?

Carbon nanotubes: probes for the present and future

Carbon nanotubes are materials that can overcome limitations that have hampered the use of AFM in structural biology. Nanotubes consist of seamless cylinders made from sp^2-bonded carbon (Figure 2a) that can be microns

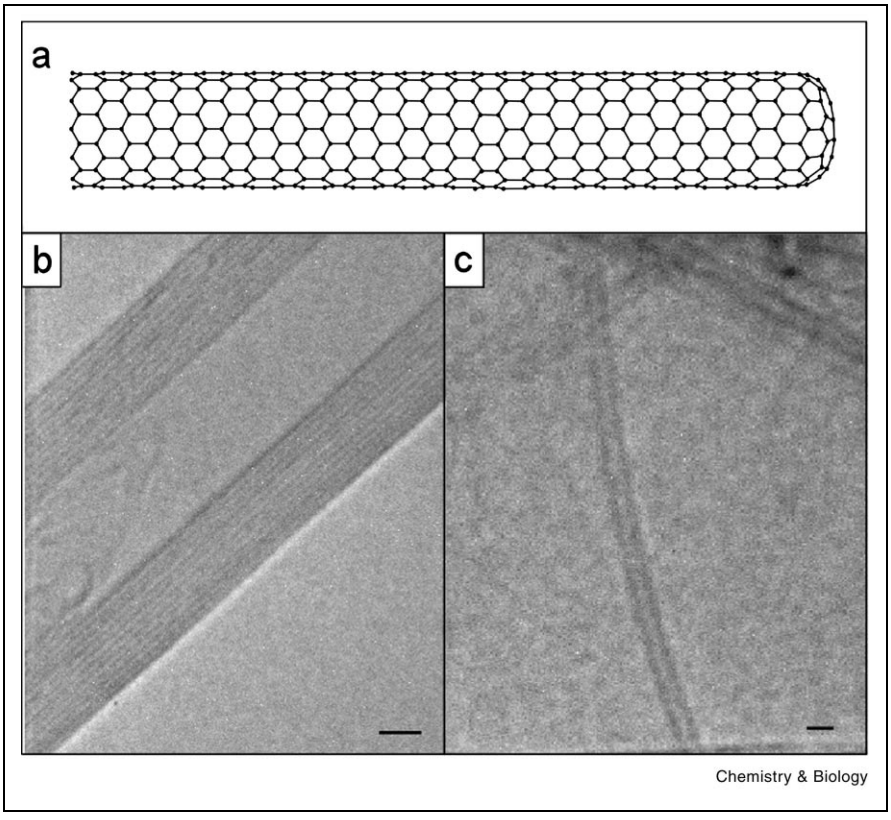

Figure 2. Structures of carbon nanotubes. **(a)** Truncated stick model of a SWNT. Each hexagonal vertex corresponds to a sp^2-hybridized carbon atom. TEM images showing the cross-sectional structures of **(b)** a MWNT and **(c)** a SWNT (scale bar, 2 nm).

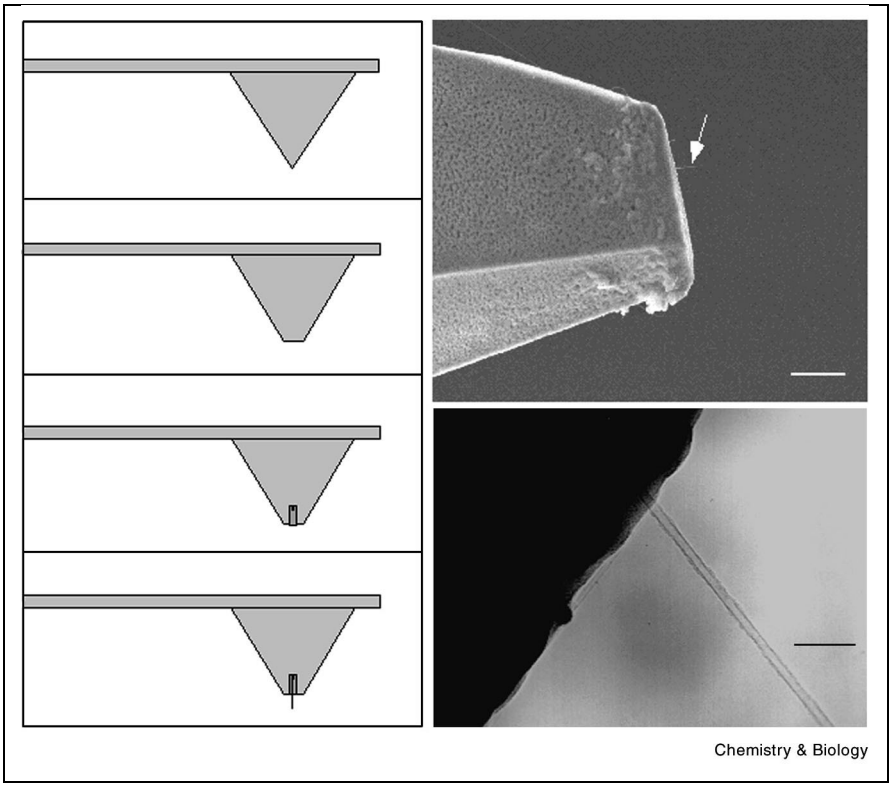

Figure 3. The pore growth technique for CVD nanotube tip fabrication. **(left)** Schematic of steps for tip fabrication: flattening, pore formation, catalyst deposition and CVD nanotube growth. SEM (**top right**, 1 μm scale bar) and TEM (**bottom right**, 20 nm scale bar) images of carbon nanotube tips made by pore growth. The white arrow in the upper image highlights the position of a ca. 500 nm long nanotube tip.

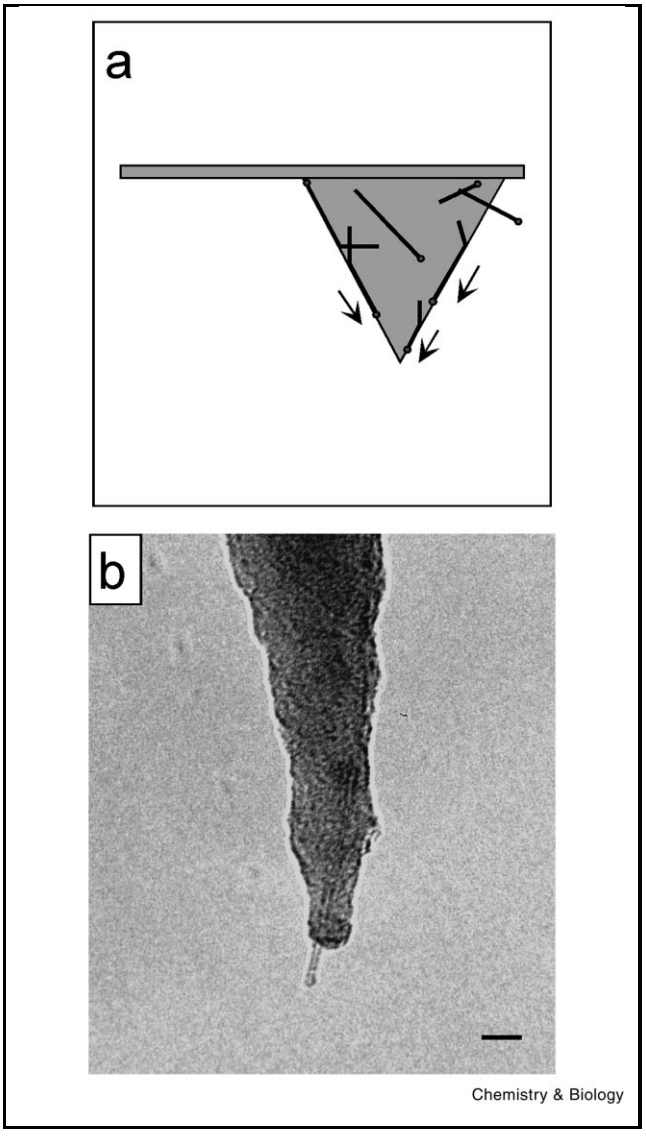

Figure 4. Surface growth CVD nanotube tip preparation. **(a)** Schematic of the surface growth process, where nanotubes grow on the surface of the pyramid, guided by the edges towards the tip apex. **(b)** TEM image of an individual SWNT tip produced by surface growth. The scale bar is 10 nm.

in length. Two distinct structural families, multi-walled nanotubes (MWNTs) and single-walled nanotubes (SWNTs) are known to exist. MWNTs typically range from 5 to 100 nm in diameter and consist of seamless concentric tubes with an intrashell spacing of 0.34 nm, while SWNTs consist of single, seamless cylinders with 0.7–5 nm diameters. Figure 2b,c shows TEM images of a MWNT and SWNT, respectively. The small radii and high aspect ratio of SWNTs make them intriguing candidates for AFM tips, although two additional properties of nanotubes, extremely large Young's modulus (stiffness) and the

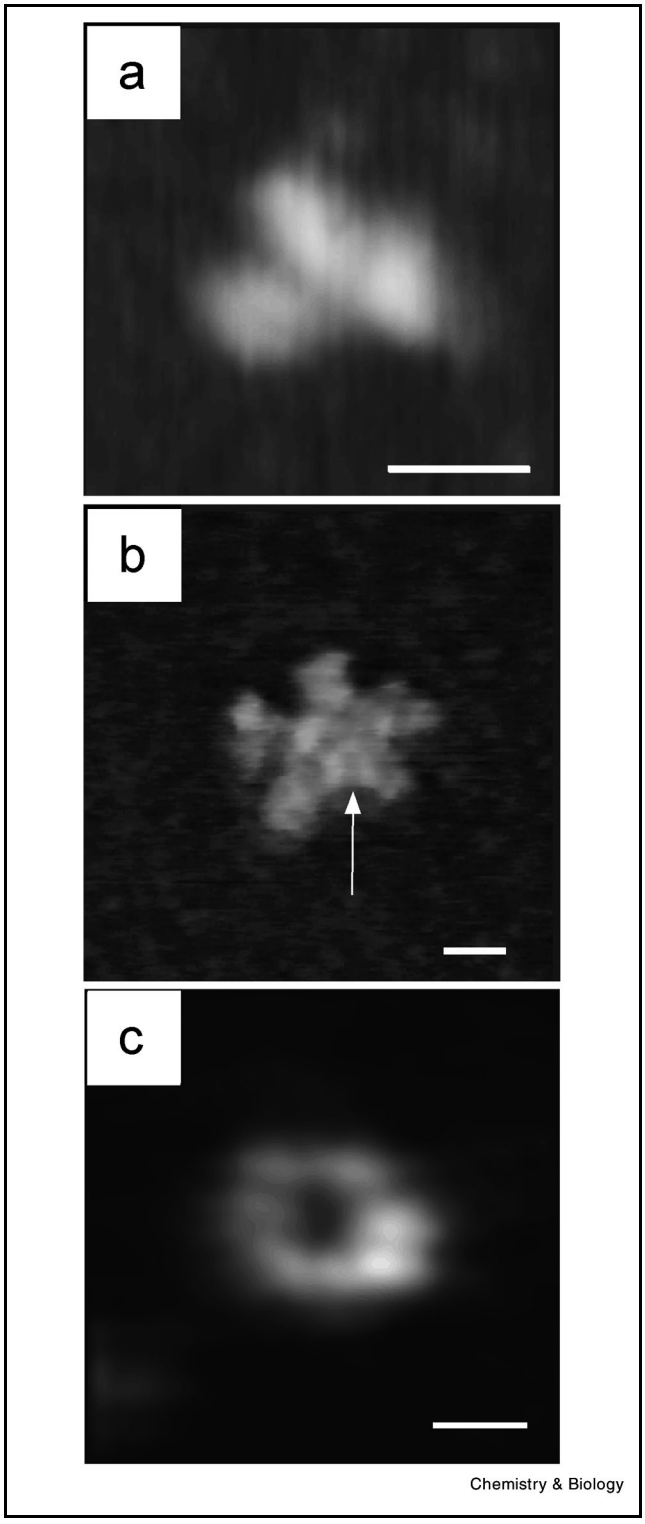

Figure 5. High-resolution protein imaging with nanotube tips. **(a)** Isolated IgG molecule imaged with a pore growth MWNT tip. **(b)** Single IgM molecule observed with a pore growth MWNT tip. The white arrow highlights the location of the joining loop. **(c)** Individual GroES molecule detected with a surface growth SWNT tip. Scale bars correspond to 10 nm in **(a)** and **(b)**, and 5 nm in **(c)**.

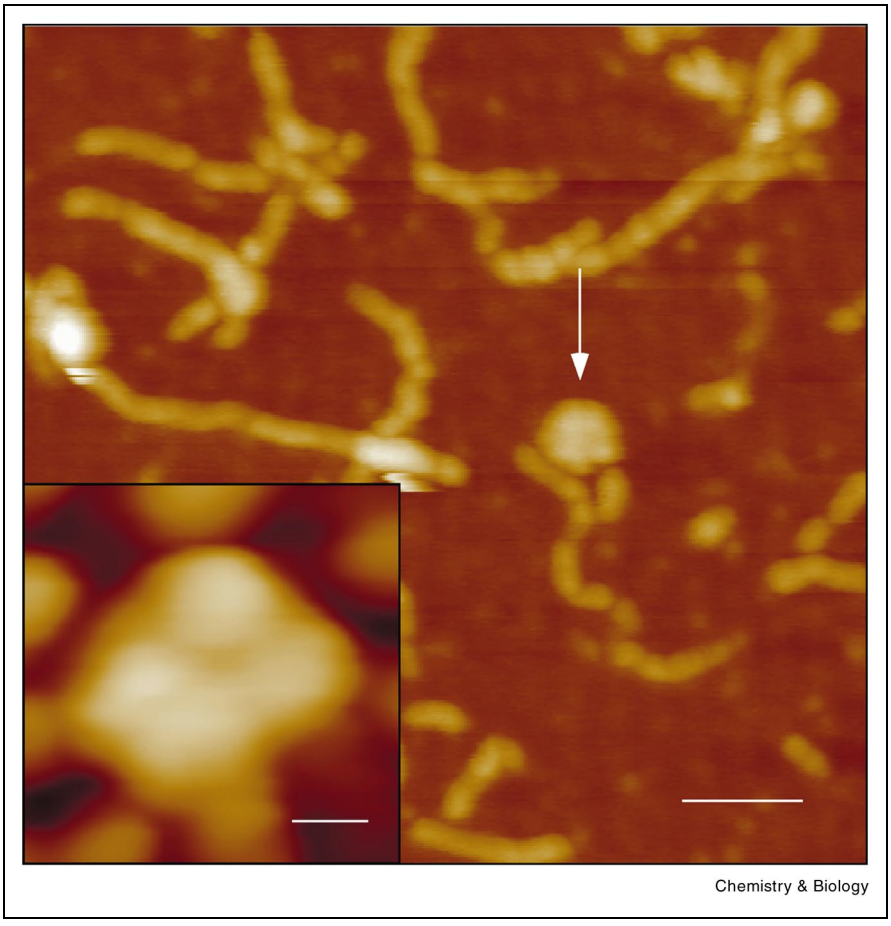

Figure 6. SWNT tip AFM images of Aβ aggregates. An Aβ annular structure, indicated by the white arrow is seen among amyloid protofibrils deposited on mica; scale bar is 50 nm. **(inset)** High-resolution image of an Aβ annular structure; scale bar is 5 nm.

ability to buckle elastically under large loads are essential to their use as probe tips. The calculated [17] and experimentally measured [18,19] Young's moduli of SWNTs and MWNTs are on the order of 1–1.3 TPa, making nanotubes the stiffest materials known to man. This stiffness makes finite length nanotubes less susceptible to thermal vibration, which would degrade resolution. The fact that carbon nanotubes buckle elastically – much like a plastic drinking straw – under large loads [18,20,21] and do not fracture or plastically deform like Si and Si_3N_4 also makes them mechanically robust, even for diameters smaller than individual proteins.

The first demonstration of nanotube probes used mechanical mounting of bundles of MWNTs onto standard AFM tips [21]. AFM studies with mechanically mounted MWNT probes yielded only modest improvements in resolution on amyloid fibrils, protofibrils, and gold nanocluster standards with respect to standard Si tips [22]. In contrast, probes fabricated from etched SWNT bundles, which occasionally have just a few SWNTs protruding from the end, demonstrated up to fivefold better resolution than conventional probes on inorganic nanostructures and DNA [22,23]. While these results indicated the potential for SWNTs to enhance AFM resolution, tip radii were still 10 times larger than what would be obtained with a single 0.25 nm radius nanotube [24]. Moreover, the conceptual simplicity of mechanical nanotube tip fabrication is hampered by its difficulty in scale-up and by its intrinsic selectivity towards thicker nanotube bundles. Mechanical nanotube tip assembly in a scanning electron microscope (SEM) [25] allows assembly of somewhat smaller >10 nm diameter tips, but this method is even slower than mounting in an optical microscope. Thus, a different approach is needed for reproducible and scaleable fabrication of ultra-high resolution nanotube tips.

Direct synthesis of nanotube probe tips

All of the problems associated with manual assembly can be solved by directly growing nanotubes on AFM tips using metal-catalyzed chemical vapor deposition (CVD). By carefully manipulating CVD reaction conditions and the catalyst, one can selectively produce SWNTs [26] with radii as small as 0.35 nm [27]. For CVD fabrication of nanotube probes, two key considerations must be addressed: (1) the nanotube tip must grow in an orientation

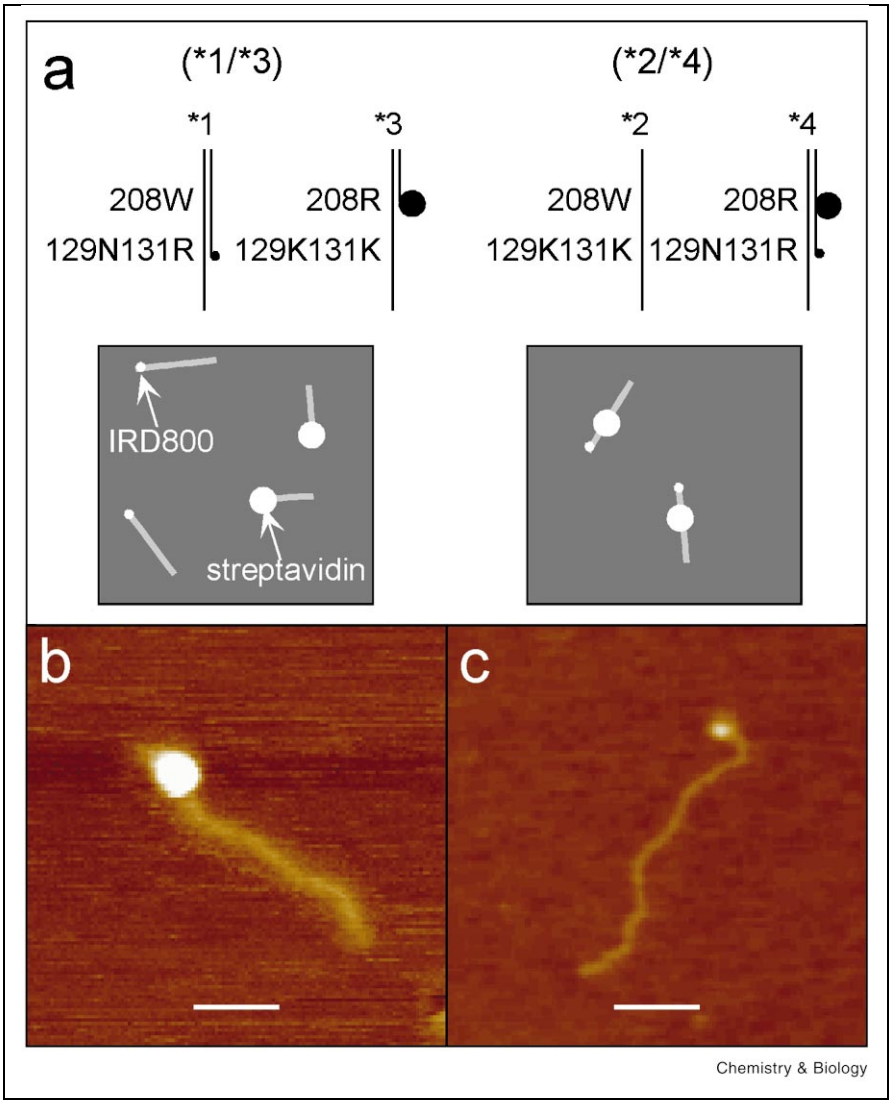

Figure 7. Direct haplotyping of UGT1A7 using SWNT probes. **(a)** Schematic showing two distinct haplotypes and the corresponding four alleles arising from the two polymorphic sites on the UGT1A7 gene. The *1/*3 haplotype denotes the two alleles (208W, 131R) and (208R, 131K), while the *2/*4 haplotype denotes the two alleles (208W, 131K) and (208R, 131R), where W, R and K denote the amino acid encoded by the DNA. The enzyme encoded by *4 allele, which is not compensated by the *2 allele, leads to an increased cancer risk factor. Since the genotypes corresponding to the heterozygous *1/*3 and *2/*4 haplotypes are the same, the risk factor can only be determined by identifying the haplotype. The binding locations of oligonucleotide probe molecules with single base sensitivity specifically label at the 129N131R and 208R sites with IRD800 (small filled circle) and streptavidin (large filled circle), respectively. Expected AFM images of a (*1/*3) sample should consist of nearly the same number of ~210 nm IRD800 end-labeled fragments and ~140 nm streptavidin end-labeled molecules (bottom left **(a)**). In contrast, a (*2/*4) sample should have ~210 nm fragments with IRD800 at one end and streptavidin 70 nm distant. Representative SWNT bundle tip AFM images of the *3 allele **(b)** and the *1 allele **(c)**, obtained from a sample with the (*1/*3) haplotype. These images show directly the single streptavidin **(b)** and IRD800 **(c)** labels that enable direct allele and haplotype identification for the sample. Scale bars are 50 nm.

perpendicular to the surface, and (2) growth should produce controlled diameter nanotubes at the tip apex. We have developed two general approaches for direct growth of nanotube tips by CVD, which overcome the above two issues; these are 'pore growth' [28,29] and 'surface growth' [30,31].

The pore growth method utilizes nanopores created at the tip apex – for example by chemical etching or focused ion beam milling – to guide the growth of nanotube probes in an orientation ideal for imaging (Figure 3). Electrochemically or electrophoretically deposited iron in the nanopores catalyzes the selective CVD growth of nanotubes with an orientation controlled by the pores [28,29]. Tips synthesized using the electrochemically deposited iron catalyst were shown to consist reproducibly of individual 3–5 nm radii MWNTs oriented optimally for high-resolution imaging (Figure 3) [28]. Significantly, these studies demonstrated for the first time that a well-defined synthetic approach could be used to prepare directly nanotube probes, thus opening the possibility of precise control over nanotube size and thereby tip resolution. A recent demonstration of this key point is the reproducible growth of SWNT tips having much smaller radii of only 1–3 nm using well-defined iron oxide nanocluster catalysts [29]. These latter tips begin to approach the theoretical minimum size expected for individual SWNTs.

The surface growth method represents an attractive alternative to the above pore growth approach in that it exploits the power and control of CVD synthesis for nanotube tip preparation but dispenses with the need to create nanopores [30,31]. In the surface growth method, competing nanotube-surface and nanotube bending energies self-di-

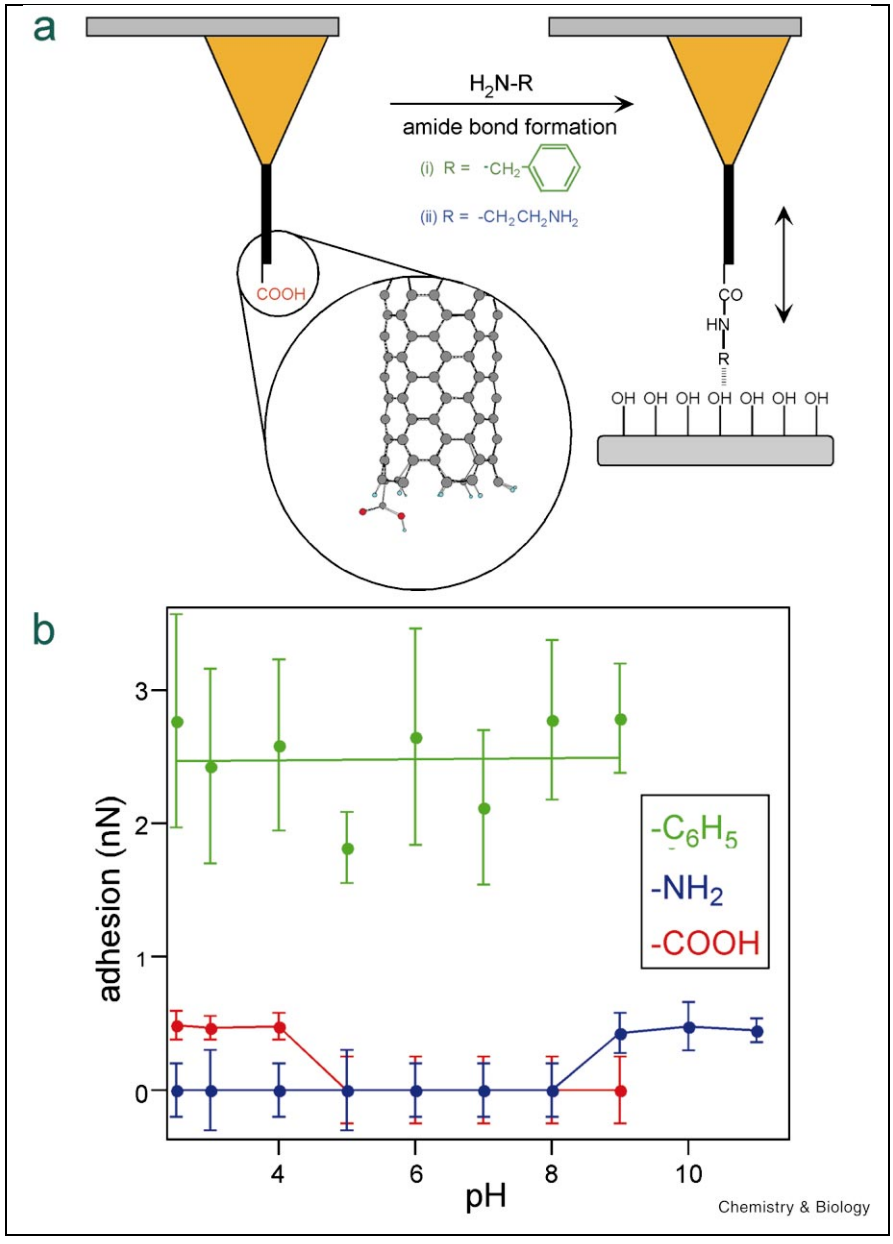

Figure 8. Chemical functionalization of nanotube tips. **(a)** Schematic of the opened end of an oxidized nanotube tip and the carbodiimide coupling chemistry used in derivatization. **(b)** Adhesion plotted as a function of pH between functionalized SWNT bundle tips and an OH-terminated SAM surface on Au. **Red:** – COOH tip; **green:** – C_6H_5 tip; **blue:** – NH_2 tip.

rect the tip orientation during synthesis (Figure 4a). A growing nanotube that reaches the pyramid edge at a glancing angle will bend if the attractive nanotube–surface interaction exceeds the energetic cost for bending. After bending the growing tube will follow the pyramid edge to the apex where it protrudes in an orientation ideal for imaging (Figure 4). Electron microscopy studies have verified the essential details and reproducibility of the surface growth approach [30,31], and moreover, have shown that by lowering the catalyst density it is possible to produce well-defined individual SWNT tips, as shown in Figure 4b [31]. These studies have demonstrated the power of synthesis for controlling in a predictable manner the size of AFM tips at the molecular scale, and thus we believe represent a true breakthrough for AFM imaging in biology. In addition, it is worth noting that these CVD tip growth methods are scaleable, in contrast to mechanical mounting, and could be implemented for large-scale production of AFM probes with sub-nanometer resolution.

Structural imaging

The ideal geometry of carbon nanotube tips, which is exemplified by the above electron micrographs, can improve resolution significantly in AFM. Images of monodisperse, incompressible 5.7 nm diameter colloidal Au particles [32] indicated tip radii [33] as small as 6 and 3 nm

for mechanically mounted MWNT and SWNT bundles, respectively [23]; similarly, pore growth MWNT and SWNT bundle tips had radii from 3 to 6 and 2 to 4 nm, respectively [29]. Importantly, these nanotube tips provided high resolution on structures ~6 nm tall, rather than on sub-nanometer corrugations that have been well resolved occasionally with fragile asperities on conventional tips.

The improved resolution of nanotube tips is clearly demonstrated in AFM images of isolated proteins. Immunoglobulin G (IgG), a ~150 kDa protein comprised of four polypeptide chains, has a 'Y' shaped structure [34], although most prior attempts to image IgG with AFM yielded only a heart-shaped structure at room temperature [35], or a Y shape at cryogenic temperatures [36]. In contrast, IgG molecules imaged at room temperature with pore growth MWNT tips exhibited reproducibly the distinct Y structure with resolution consistent with independent assessment of the tip radii (Figure 5a) [29]. These individual MWNT tips were also used to resolve the five subunits of immunoglobulin M (IgM) in AFM images, and even showed evidence for the joining loop structure that links two of the five central domains (Figure 5b) [28]. This represents a clear example of the potential for nanotube probes to impact structural biology, as the crystal structure of IgM has thus far eluded researchers. A final system that showcases the enhanced resolution of nanotube probes is GroES, whose crystal structure indicates an 8 nm diameter hollow dome-shaped heptamer [37]. Significantly, the improved resolution of SWNT probes allowed imaging of two conformations of isolated GroES molecules for the first time: a ring-like structure with an 11 nm outer diameter and heptameric symmetry (Figure 5c), and a dome-shaped structure of the same diameter [29]; these distinct structures correspond to the two sides of the GroES heptamer.

The ability to synthesize reproducible, high-resolution nanotube probes enables the de novo study of the structures uncharacterized biological systems. For instance, previous AFM studies of the formation of amyloid-β (Aβ) fibrils, which are a defining pathological feature of Alzheimer's disease, revealed that fibrils formed from an unanticipated intermediate, the Aβ protofibril [38]. These studies [38] also indicated the presence of smaller, globular Aβ oligomers at early stages of aggregation, although the

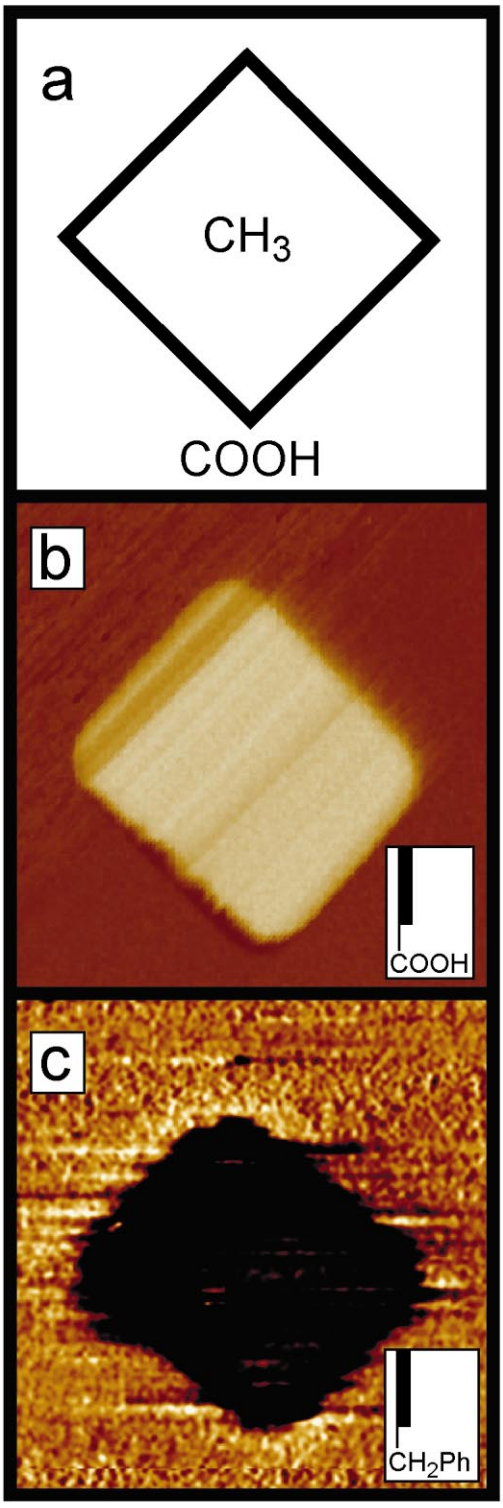

→

Figure 9. Chemically sensitive imaging with functionalized nanotube tips. **(a)** Schematic of a patterned SAM terminating in methyl (CH_3) and carboxyl (COOH) end groups. **(b)** Tapping mode phase image [53] of the patterned SAM shown in **(a)** obtained with a COOH-terminated tip. **(c)** Phase image of a similar sample using a C_6H_5-terminated tip. The inversion of contrast with tip functionality confirms the chemical mapping.

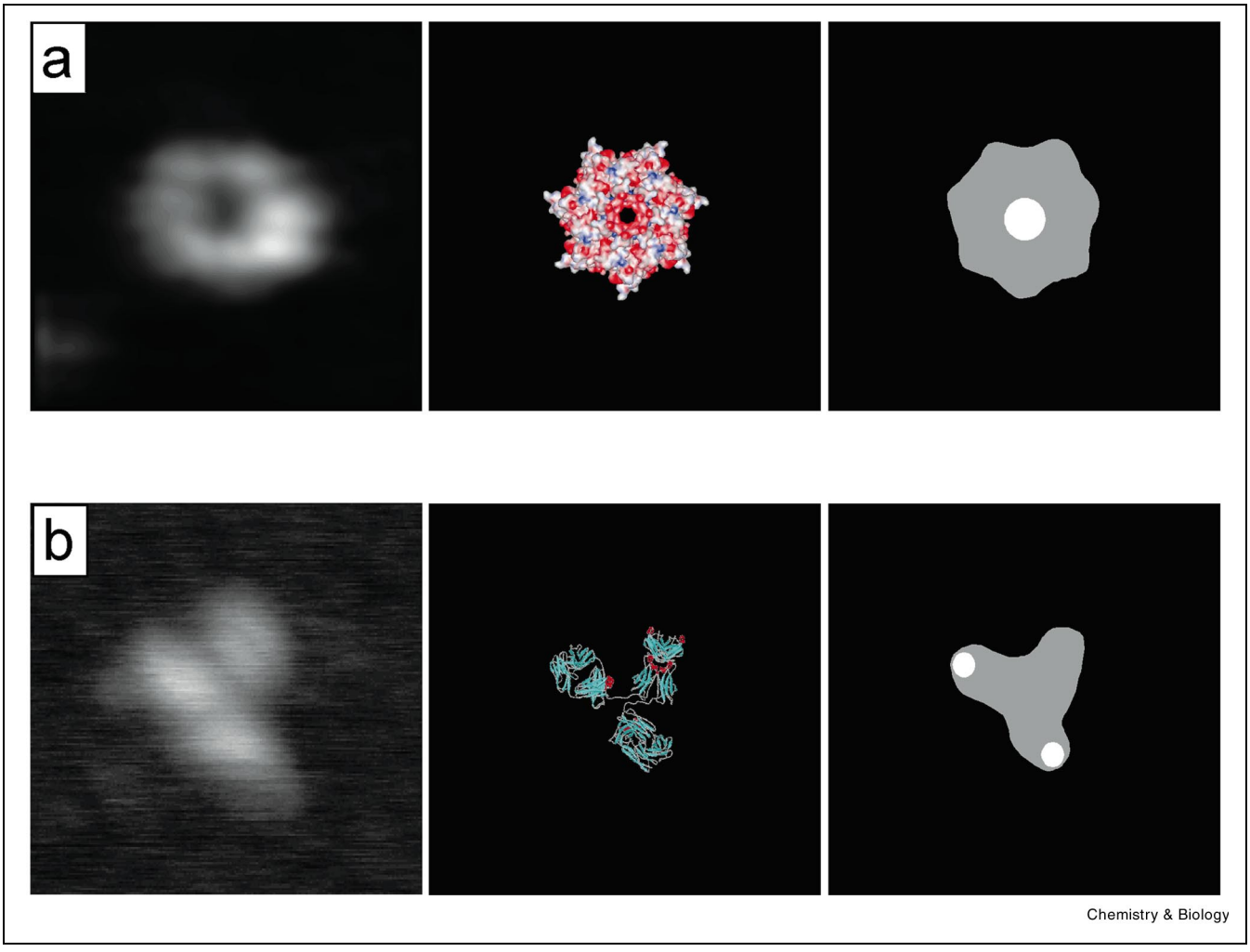

Figure 10. Mapping domains in proteins. **(a)** GroES topograph obtained with SWNT tip **(left)** and crystal structure **(middle)**. The expected phase image obtained with a carboxy-terminated tip **(right)** shows a repulsive region (filled white circle) at the GroES center. **(b)** IgG topograph **(left)**, crystal structure **(middle)** and the expected phase image obtained with modified SWNT tip **(right)**. The two filled white circles highlight the antigen binding sites.

conventional tips used for imaging were too large to provide detailed structural information about such small oligomers. In contrast, recent investigations using ultrahigh resolution CVD SWNT probes have led to the discovery that some of the 'globular' Aβ oligomers have annular structures with fourfold internal symmetry and a central pore-like depression (Figure 6) [39]. This new result is especially intriguing in light of reports that a small, nonfibrillar form of Aβ may be responsible for neurodegeneration in Alzheimer's disease [40,41].

Another area where nanotube probes have the potential to impact significantly is DNA analysis. Indeed, these tips have recently been used for multiplex detection of sequence specific labels at polymorphic sites in DNA fragments [42]. This powerful methodology has also been applied to the determination of haplotypes – the specific alleles associated with each chromosome homologue – in the model gene UGT1A7, which is under study as a cancer risk factor [43]. UGT1A7 has two polymorphic sites 233 bases apart, which determine four alleles, each specifying alternative polypeptide chains (Figure 7a). Individuals who are heterozygous at both loci have the same genotype, but one of two haplotypes, (*1/*3) or (*2/*4), which cannot be differentiated by conventional methods. This ambiguity is critical in screening, since each allele exhibits substantially different activity towards targeted carcinogens. Importantly, the haplotypes of several subject samples were unambiguously determined to be (*1/*3) by direct inspection of SWNT tip images (Figure 7b,c) [42]. Direct haplotyping with SWNT tips represents a significant advance over conventional approaches and could facilitate high-throughput

screening of single nucleotide polymorphisms for association and linkage studies of inherited diseases and genetic risk. These promising new results in amyloid characterization and haplotyping are a harbinger of the wealth of structural information that can be obtained using the enhanced resolution provided by nanotube probes.

Functional imaging

Perhaps the greatest impact of nanotube probes on structural biology will come from combining their sub-nanometer resolving power with chemically sensitive imaging in chemical force microscopy (CFM) [44]. While previous CFM work has demonstrated the attachment of controlled functional groups [44–48] or even single molecules [15,16] to conventional AFM tips, the spatial resolution of this methodology was limited to ≥10 nm using conventional silicon and silicon nitride tips. However, carbon nanotubes offer the unique potential to overcome this disadvantage because of their small radii and the distinct difference in reactivity between the nanotube ends and side-walls, which enables well-defined localization of molecules at the tip end [49].

Spectroscopic studies of oxidized bulk MWNTs indicated the presence of carboxylic acid groups (COOH) [50], which were proposed also to exist at opened nanotube ends (Figure 8a). Indeed, adhesion measurements taken as a function of pH (force titrations [47,48]) between MWNT or SWNT tips and non-ionizable hydroxyl (OH)-terminated SAMs confirmed that nanotube tips terminate with COOH (Figure 8b) [49,51]. These terminal COOH have been coupled with amine-containing moieties to form amide bonds and generate nanotubes that end with phenyl or amine functionality, where the presence of these groups was verified by force titrations (Figure 8b) [49,51]. As an alternative to solution chemistry, nanotubes also have been functionalized using gases activated by a transient arc at the tip end. For example, COOH-terminated nanotubes were produced from O_2, while nanotubes reacted in pure

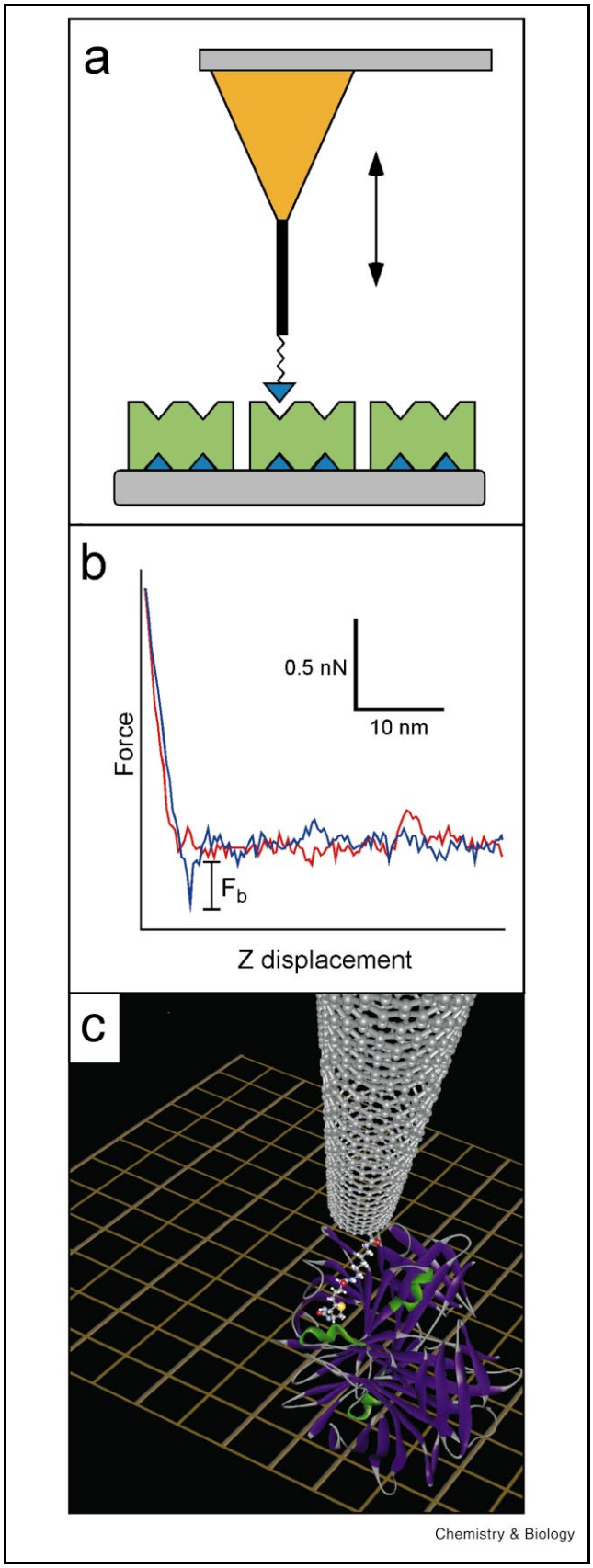

→

Figure 11. Single-molecule force spectroscopy with nanotube tips. **(a)** Schematic experimental illustration; the lower gray rectangle represents a mica substrate, the green blocks correspond to streptavidin and the dark blue inverted triangle is biotin covalently attached to a nanotube tip (thick black vertical line). **(b)** Representative force–displacement curve obtained with a biotin-modified nanotube tip on a streptavidin surface in solution. The red curve corresponds to the approach of the biotin-labeled tip to the streptavidin receptor, and the blue curve corresponds to the subsequent separation of the labeled tip from the protein. The new feature in the separation (blue) curve corresponds to the unbinding of a single biotin ligand from the streptavidin binding site. The force required to unbind the biotin ligand is denoted F_b. **(c)** To scale model of a SWNT tip that has been modified with biotin and is interacting with streptavidin.

H_2 exhibited pH independent behavior, and nanotubes reacted in pure N_2 demonstrated basic properties [52].

These studies clearly demonstrate considerable flexibility with regards to the localization of chemical functionality at the ends of nanotube probes. Importantly, the reproducible synthesis of chemically well-defined nanotube tips enables significantly improved lateral resolution in CFM. We have shown that just like conventional functionalized silicon and silicon nitride tips [53], MWNT [49] and SWNT tips [51] can distinguish between regions of different chemical functionality on surfaces (Figure 9), but with improved spatial resolution. Indeed, 'chemical resolution' as good as 3 nm for SWNT bundle tips was obtained on partial bilayer surfaces [51], and recent CFM results with CVD grown individual SWNT tips [54] indicate the potential for sub-nanometer 'chemical resolution'.

Chemically well defined, nanotube probes will enable sub-nanometer mapping of chemical domains and binding sites on proteins and protein complexes. For example, GroES, which has been resolved at the subunit level with our SWNT tips [37], could serve as a model system for such studies because the crystal structure indicates a high density of acidic residues at the top of its dome structure (Figure 10a). Hence, CFM at neutral pH with COO^--terminated nanotube tips should readily sense a region of repulsive potential on the dome of GroES as indicated schematically in Figure 10a. Furthermore, the reactive sites at nanotube ends can be modified to study ligand–receptor interactions with sub-nanometer resolution on proteins or cells. Indeed, we have examined the model ligand–receptor system biotin–streptavidin [55], by attaching biotin functionality to nanotube tips and characterizing the adhesion force between tip-bound biotin and surface streptavidin (Figure 11a) [49]. Force spectroscopy measurements exhibited well-defined binding force quanta of $\sim$200 pN per biotin–streptavidin pair (Figure 11b). These results demonstrate that a single, active ligand can be localized precisely and controllable at the tip of a nanotube with nanometer-scale precision (Figure 11c), a significant advantage compared to earlier work using biotin or streptavidin attached on lower resolution tips [56,57]. Moreover, the present availability of individual CVD grown SWNT probes makes it reasonable to consider spatially mapping ligand binding sites on a wide range of proteins. As an example, the reproducible subunit structural resolution obtained on IgG could be extended significantly with modified tips to map the two antigen binding sites as shown in Figure 10b.

Future prospects

The ideal geometry, mechanical and chemical properties of carbon nanotube probes overcome the limitations of Si and Si_3N_4 tips and offer reproducible sub-nanometer resolution imaging of biomolecules. Development of facile methods for direct CVD growth of nanotube tips enables predictable synthesis of individual SWNT probes and provides a scaleable approach for making such tips widely available to structural biologists. Nanotube technology will facilitate significant advances in AFM, just as improvements in electron and X-ray sources have furthered electron microscopy and diffraction techniques. Current progress indicates that SWNT tips will provide sub-nanometer structural resolution on proteins in solution, and functionalized tips will allow high-resolution mapping of binding sites and chemically distinct domains on biomolecules. Thus, we believe that SWNT probes will enable an essentially unlimited range of experiments in the future, which will contribute valuable new information about the structure and function of complex protein and protein–nucleic acid assemblies.

Acknowledgements

C.M.L. acknowledges support of this work by the Air Force Office of Scientific Research and the National Institutes of Health. A.T.W. acknowledges fellowship support from the Cancer Research fund of the Damon Runyon-Walter Winchell Foundation. J.H.H. was supported by a postdoctoral training grant from the National Institutes of Health.

References

1. Glusker, J.P. (1994). X-ray crystallography of proteins. *Methods Biochem. Anal.* **37**, 1–72.
2. Henderson, R. (1995). The potential and limitations of neutrons, electrons and X-rays for atomic resolution microscopy of unstained biological molecules. *Quart. Rev. Biophys.* **28**, 171–193.
3. Wuthrich, K. (1995). NMR: This other method for protein and nucleic acid structure determination. *Acta Cryst. D* **51**, 249–270.
4. Beauchamp, J.C. & Isaacs, N.W. (1999). Methods for X-ray diffraction analysis of macromolecular structures. *Curr. Opin. Chem. Biol.* **3**, 525–529.
5. Glaeser, R.M. (1999). Review: Electron crystallography: Present excitement, a nod to the past, anticipating the future. *J. Struct. Biol.* **128**, 3–14.
6. Siegal, G., van Duynhoven, J. & Baldus, M. (1999). Biomolecular NMR: Recent advances in liquids, solids and screening. *Curr. Opin. Chem. Biol.* **3**, 530–536.
7. Kim, S.H. (1998). Shining a light on structural genomics. *Nature Struct. Biol.* **5**, 643–645.
8. Wuthrich, K. (2000). Protein recognition by NMR. *Nature Struct. Biol.* **7**, 188–189.
9. Binnig, G., Quate, C.F. & Gerber, C. (1986). Atomic force microscope. *Phys. Rev. Lett.* **56**, 930–933.
10. Bustamante, C., Rivetti, C. & Keller, D.J. (1997). Scanning force microscopy under aqueous solutions. *Curr. Opin. Struct. Biol.* **7**, 709–716.
11. Hansma, H.G. & Pietrasanta, L. (1998). Atomic force microscopy and other scanning probe microscopies. *Curr. Opin. Chem. Biol.* **2**, 579–584.
12. Kasas, S., Thomson, N.H., Smith, B.L., Hansma, P.K., Miklossy, J. & Hansma, H.G. (1997). Biological applications of the AFM: From single molecules to organs. *Int. J. Imaging Syst. Technol.* **8**, 151–161.
13. Mou, J.X., Czajkowsky, D.M., Sheng, S.J., Ho, R.Y. & Shao, Z.F. (1996). High resolution surface structure of *E-coli* GroES oligomer by atomic force microscopy. *FEBS Lett.* **381**, 161–164.
14. Muller, D.J., Fotiadis, D., Scheuring, S., Muller, S.A. & Engel, A. (1999). Electrostatically balanced subnanometer imaging of biological specimens by atomic force microscope. *Biophys. J.* **76**, 1101–1111.
15. Marszalek, P.E., Lu, H., Li, H., Carrion-Vazquez, M., Oberhauser, A.F., Schulten, K. & Fernandez, J.M. (1999). Mechanical unfolding intermediates in titin modules. *Nature* **402**, 100–103.

16. Noy, A., Vezenov, D.V., Kayyem, J.F., Meade, T.J. & Lieber, C.M. (1997). Stretching and breaking duplex DNA by chemical force microscopy. *Chem. Biol.* **4**, 519–527.
17. Lu, J.P. (1997). Elastic properties of carbon nanotubes and nanoropes. *Phys. Rev. Lett.* **79**, 1297–1300.
18. Wong, E.W., Sheehan, P.E. & Lieber, C.M. (1997). Nanobeam mechanics: Elasticity, strength, and toughness of nanorods and nanotubes. *Science* **277**, 1971–1975.
19. Krishnan, A., Dujardin, E., Ebbesen, T.W., Yianilos, P.N. & Treacy, M.M.J. (1998). Young's modulus of single-walled nanotubes. *Phys. Rev. B* **58**, 14013–14019.
20. Iijima, S., Brabec, C., Maiti, A. & Bernholc, J. (1996). Structural flexibility of carbon nanotubes. *J. Chem. Phys.* **104**, 2089–2092.
21. Dai, H., Hafner, J.H., Rinzler, A.G., Colbert, D.T. & Smalley, R.E. (1996). Nanotubes as nanoprobes in scanning probe microscopy. *Nature* **384**, 147–150.
22. Wong, S.S., Harper, J.D., Lansbury Jr., P.T. & Lieber, C.M. (1998). Carbon nanotube tips: High resolution probes for imaging biological systems. *J. Am. Chem. Soc.* **120**, 603–604.
23. Wong, S.S., Woolley, A.T., Odom, T.W., Huang, J.-L., Kim, P., Vezenov, D.V. & Lieber, C.M. (1998). Single-walled carbon nanotube probes for high-resolution nanostructure imaging. *Appl. Phys. Lett.* **73**, 3465–3467.
24. Sun, L.F., Xie, S.S., Liu, W., Zhou, W.Y., Liu, Z.Q., Tang, D.S., Wang, G. & Qian, L.X. (2000). Creating the narrowest carbon nanotubes. *Nature* **403**, 384.
25. Nishijima, H., Kamo, S., Akita, S., Nakayama, Y., Hohmura, K.I., Yoshimura, S.H. & Takeyasu, K. (1999). Carbon-nanotube tips for scanning probe microscopy: Preparation by a controlled process and observation of deoxyribonucleic acid. *Appl. Phys. Lett.* **74**, 4061–4063.
26. Hafner, J.H., Bronikowski, M.J., Azamian, B.R., Nikolaev, P., Rinzler, A.G., Colbert, D.T., Smith, K.A. & Smalley, R.E. (1998). Catalytic growth of single-wall carbon nanotubes from metal particles. *Chem. Phys. Lett.* **296**, 195–202.
27. Nikolaev, P., Bronikowski, M.J., Bradley, R.K., Rohmund, F., Colbert, D.T., Smith, K.A. & Smalley, R.E. (1999). Gas-phase catalytic growth of single-walled carbon nanotubes from carbon monoxide. *Chem. Phys. Lett.* **313**, 91–97.
28. Hafner, J.H., Cheung, C.L. & Lieber, C.M. (1999). Growth of nanotubes for probe microscopy tips. *Nature* **398**, 761–762.
29. Cheung, C.L., Hafner, J.H. & Lieber, C.M. (2000). Carbon nanotube atomic force microscopy tips: Direct growth by chemical vapor deposition and application to high resolution imaging. *Proc. Natl. Acad. Sci. USA* **97**, 3809–3813.
30. Hafner, J.H., Cheung, C.L. & Lieber, C.M. (1999). Direct growth of single-walled carbon nanotube scanning probe microscopy tips. *J. Am. Chem. Soc.* **121**, 9750–9751.
31. Cheung, C.L., Hafner, J.H., Odom, T.W., Kim, K. & Lieber, C.M. (2000). Growth and fabrication with single-walled carbon nanotube probe microscopy tips. *Appl. Phys. Lett.* **76**, 3136–3138.
32. Vesenka, J., Manne, S., Giberson, R., Marsh, T. & Henderson, E. (1993). Colloidal gold particles as an incompressible atomic force microscope imaging standard for assessing the compressibility of biomolecules. *Biophys. J.* **65**, 992–997.
33. Bustamante, C., Keller, D. & Yang, G.L. (1993). Scanning force microscopy of nucleic acids and nucleoprotein assemblies. *Curr. Opin. Struct. Biol.* **3**, 363–372.
34. Silverton, E.W., Navia, M.A. & Davies, D.R. (1977). Three-dimensional structure of an intact human immunoglobulin. *Proc. Natl. Acad. Sci. USA* **74**, 5140–5144.
35. Fritz, J., Anselmetti, D., Jarchow, J. & Fernàndez-Busquets, X. (1997). Probing single biomolecules with atomic force microscopy. *J. Struct. Biol.* **119**, 165–171.
36. Zhang, Y.Y., Sheng, S.T. & Shao, Z.F. (1996). Imaging biological structures with the cryo atomic force microscope. *Biophys. J.* **71**, 2168–2176.
37. Sigler, P.B., Xu, Z.H., Rye, H.S., Burston, S.G., Fenton, W.A. & Horwich, A.L. (1998). Structure and function in GroEL-mediated protein folding. *Annu. Rev. Biochem.* **67**, 581–608.
38. Harper, J.D., Wong, S.S., Lieber, C.M. & Lansbury Jr., P.T. (1997). Observation of metastable Aβ amyloid protofibrils by atomic force microscopy. *Chem. Biol.* **4**, 119–125.
39. Hafner, J.H., Harper, J.D., Lansbury, P.T., Jr. & Lieber, C.M. (2000). Aβ40 annular structure revealed by high-resolution carbon nanotube probe tips, manuscript in preparation.
40. Moechars, D., Dewachter, I., Lorent, K., Reverse, D., Baekelandt, V., Naidu, A., Tesseur, I., Spittaels, K., Van Den Haute, C., Checler, F., Godaux, E., Cordell, B. & Van Leuven, F. (1999). Early phenotypic changes in transgenic mice that overexpress different mutants of amyloid precursor protein in brain. *J. Biol. Chem.* **274**, 6483–6492.
41. Hsia, A.Y., Masliah, E., McConlogue, L., Yu, G.Q., Tatsuno, G., Hu, K., Kholodenko, D., Malenka, R.C., Nicoll, R.A. & Mucke, L. (1999). Plaque-independent disruption of neural circuits in Alzheimer's disease mouse models. *Proc. Natl. Acad. Sci. USA* **96**, 3228–3233.
42. Woolley, A.T., Guillemette, C., Cheung, C.L., Housman, D.E. & Lieber, C.M. (2000). Direct haplotyping of kilobase-size DNA using carbon nanotube probes. *Nature Biotechnol.* **18**, 760–763.
43. Guillemette, C., Ritter, J.K., Auyeung, D.J., Kessler, F.K. & Housman, D.E. (2000). Structural heterogeneity at the UDP-glucuronosyltransferase 1 locus: Functional consequences of three novel missense mutations in the human UGT1A7 gene. *Pharmacogenetics* **10**, 629–644.
44. Frisbie, C.D., Rozsnyai, L.F., Noy, A., Wrighton, M.S. & Lieber, C.M. (1994). Functional group imaging by chemical force microscopy. *Science* **265**, 2071–2074.
45. Green, J.-B.D., McDermott, M.T., Porter, M.D. & Siperko, L.M. (1995). Nanometer-scale mapping of chemically distinct domains at well-defined organic interfaces using frictional force microscopy. *J. Phys. Chem.* **99**, 10960–10965.
46. Noy, A., Frisbie, C.D., Rozsnyai, L.F., Wrighton, M.S. & Lieber, C.M. (1995). Chemical force microscopy: exploiting chemically modified tips to quantify adhesion, friction, and functional group distributions in molecular assemblies. *J. Am. Chem. Soc.* **117**, 7943–7951.
47. Vezenov, D.V., Noy, A., Rozsnyai, L.F. & Lieber, C.M. (1997). Force titrations and ionization state sensitive imaging of functional groups in aqueous solutions by chemical force microscopy. *J. Am. Chem. Soc.* **119**, 2006–2015.
48. Noy, A., Vezenov, D.V. & Lieber, C.M. (1997). Chemical force microscopy. *Annu. Rev. Mater. Sci.* **27**, 381–421.
49. Wong, S.S., Joselevich, E., Woolley, A.T., Cheung, C.L. & Lieber, C.M. (1998). Covalently functionalized nanotubes as nanometre-sized probes in chemistry and biology. *Nature* **394**, 52–55.
50. Hiura, H., Ebbesen, T.W. & Tanigaki, K. (1995). Opening and purification of carbon nanotubes in high yields. *Adv. Mater.* **7**, 275–276.
51. Wong, S.S., Woolley, A.T., Joselevich, E., Cheung, C.L. & Lieber, C.M. (1998). Covalently functionalized single-walled carbon nanotube probe tips for chemical force microscopy. *J. Am. Chem. Soc.* **120**, 8557–8558.
52. Wong, S.S., Woolley, A.T., Joselevich, E. & Lieber, C.M. (1999). Functionalization of carbon nanotube AFM probes using tip-activated gases. *Chem. Phys. Lett.* **306**, 219–225.
53. Noy, A., Sanders, C.H., Vezenov, D.V., Wong, S.S. & Lieber, C.M. (1998). Chemically sensitive imaging in tapping mode by chemical force microscopy: Relationship between phase lag and adhesion. *Langmuir* **14**, 1508–1511.
54. Cheung, C.L., Chen, L. and Lieber, C.M. (2000). unpublished results.
55. Livnah, O., Bayer, E.A., Wilchek, M. & Sussman, J.L. (1993). Three-dimensional structures of avidin and the avidin–biotin complex. *Proc. Natl. Acad. Sci. USA* **90**, 5076–5080.
56. Florin, E.-L., Moy, V.T. & Gaub, H.E. (1994). Adhesion forces between individual ligand-receptor pairs. *Science* **264**, 415–417.
57. Lee, G.U., Kidwell, D.A. & Colton, R.J. (1994). Sensing discrete streptavidin–biotin interactions with atomic force microscopy. *Langmuir* **10**, 354–357.